Effects of alloy 718 microstructure on hydrogen embrittlement susceptibility for oil and gas environments

B. Kagay*[1], K. Findley[1], S. Coryell[2] and A. B. Nissan[3]

The effects of alloy 718 microstructure on hydrogen embrittlement susceptibility and tensile fracture mode were assessed through slow strain rate tensile testing and fracture surface analysis. Alloy 718 was annealed and aged to produce microstructures with variations in grain size and amount of grain boundary precipitates. Furthermore, the different ageing conditions likely resulted in differences in volume fractions and sizes of γ′ and γ″ precipitates. The extent of grain boundary precipitation had the strongest effect on hydrogen embrittlement susceptibility, while grain size did not have any significant effect. Hydrogen embrittlement susceptibility was also correlated with differences in strength level, which was primarily controlled by the γ′ and γ″ precipitate populations.

Keywords: Precipitation hardened nickel-base superalloys, Hydrogen embrittlement, Slow strain rate testing, Fractography

Introduction

UNS N07718, hereafter referred to as alloy 718, is one of the several nickel-base corrosion-resistant alloys (CRAs) from which components used for deep-sea wells in the oil and gas industry are produced. Packers, tubing hangers, fasteners and bolting components are all fabricated from CRAs because of their high strength and resistance to general corrosion processes. Field failures of CRA components can occur due to hydrogen embrittlement caused by the uptake of hydrogen, which may be produced in several different ways in downhole environments.[1–5] In these cases, hydrogen embrittlement is an environmental cracking process by which atomic hydrogen is adsorbed on the surface of the alloy, resulting in a decrease in plasticity and/or fracture strength.

Slow strain rate (SSR) tensile testing is one of the most common methods for evaluating alloy susceptibility to hydrogen embrittlement due to the relatively short test times; however, the SSR test is a more severe test method compared with constant displacement/constant load tests because of the dynamic straining.[6] Many studies have been performed using SSR tensile testing to evaluate the susceptibility of nickel-base CRAs to embrittlement in hydrogen-rich environments,[1,3,7–16] where susceptibility is often based on a comparison of tensile properties in the presence of hydrogen and in an inert or ambient environment. While increased hydrogen embrittlement susceptibility has been correlated with increased strength,[8,15] the influence of microstructure at high strength levels is not fully understood for many nickel-base CRAs. Figure 1 shows the ratio of tensile elongation from SSR tests with cathodic polarisation (CP) versus an inert environment (total elongation ratio) plotted against room-temperature yield strength for several different Ni-base CRAs (718, 625 Plus, 925, 935, 945, 945X and C22); the data were obtained from several studies.[3,7,8,15,16] There is no clear trend between hydrogen embrittlement susceptibility and strength level, which may be affected by several factors including variations in microstructure and test methodology.

One microstructural feature that is known to increase hydrogen embrittlement susceptibility is δ-phase precipitation on grain boundaries.[1,3,10–13] However, even removing the presence of extensive δ-phase does not clarify the correlation between hydrogen embrittlement and strength level. Figure 2 is a plot of total elongation ratios versus yield strength for alloy 718 without extensive precipitation of δ-phase at the grain boundaries; the data were obtained from several different studies.[3,7,8,15,16] Again, there is no clear correlation between hydrogen embrittlement susceptibility and strength, and it is difficult to deconvolute the influence of differences in microstructures and SSR testing parameters between the studies. The SSR testing parameters for the studies in Figs. 1 and 2 are listed in Table 1.

With regards to 718, several studies have been performed to determine the effect of precipitates on hydrogen embrittlement susceptibility. For reference, a time–temperature–transformation diagram for 718 is given in Fig. 3.[17] Several other studies have shown some measured variation in precipitation behaviour of alloy 718.[18–21] The primary strengthening phases of 718 are γ′-Ni_3(Ti,Al) and metastable γ″-Ni_3Nb. Ti-rich γ′ can also be metastable

[1]Colorado School of Mines, 1500 Illinois St, Golden, CO 80401, USA
[2]Special Metals Corporation, 3200 Riverside Dr, Huntington, WV 25705, USA
[3]Chevron Energy Technology Company (ETC), 100 Chevron Way, Richmond, CA 94802, USA

*Corresponding author, email bkagay@mines.edu

Published by Taylor & Francis on behalf of the Institute
Received 29 October 2015; accepted 29 December 2015
DOI 10.1080/02670836.2016.1139225

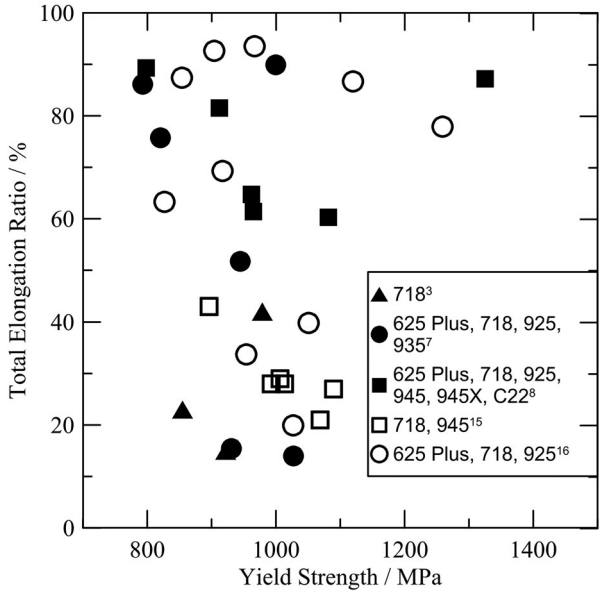

1 Ratio of elongation during cathodic hydrogen charging to elongation in an inert environment for SSR tensile tests of several different Ni-base CRAs (718, 625 Plus, 725, 925, 935, 945, 945X, C22) versus the room-temperature yield strengths of the alloys[3,7,8,15,16]

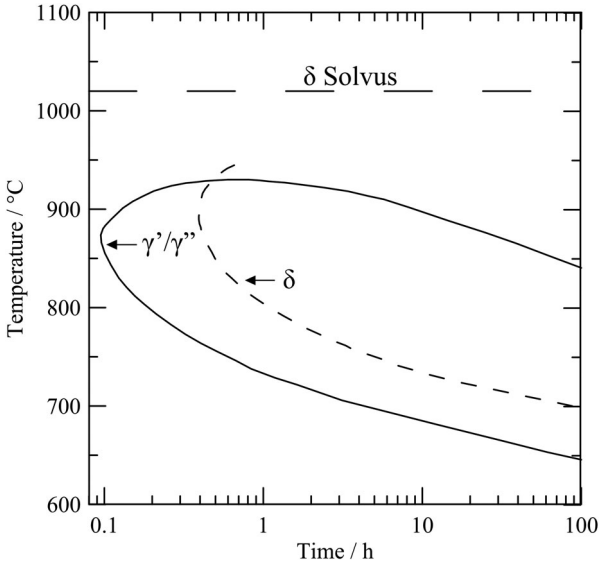

3 Time–temperature–transformation diagram for alloy 718 showing the approximate ageing temperatures and times required to precipitate the δ-phase (Ni_3Nb) and γ′-phase (Ni_3 (Ti and Al)). Adapted from Oradei-Basile and Radavich[17]

and transform to η at longer ageing times.[22] In addition to δ, other precipitates such as MC carbides, $M_{23}C_6$ carbides and Laves phase can form in alloy 718 during thermo-mechanical processing and/or heat treatment.[23] Liu *et al.*[13] found that elimination of γ′ and γ″ slightly decreases the hydrogen embrittlement susceptibility of 718, but the alloy is not used in a single phase condition because precipitate strengthening is a key component to the alloy strength.[13] On the other hand, multiple studies have found that the presence of the grain boundary strengthening δ-phase can significantly increase

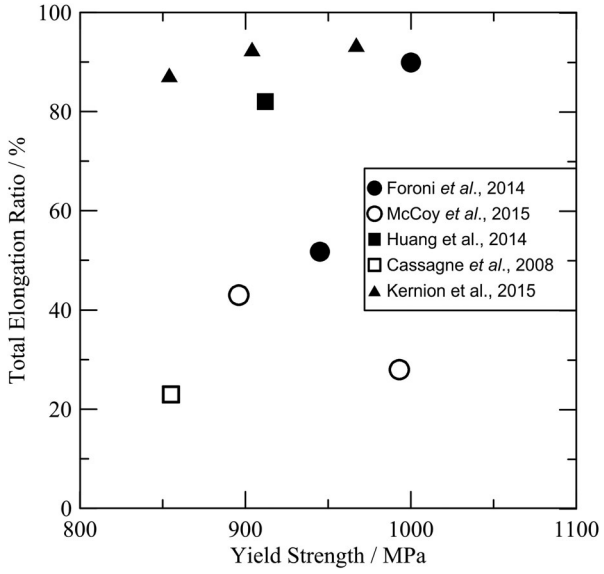

2 Ratio of elongation during cathodic hydrogen charging to elongation in an inert environment for SSR tensile tests of alloy 718 with no grain boundary δ-phase versus the room-temperature yield strength (MPa) for each of those conditions[3,7,8,15,16]

susceptibility to intergranular cracking (IGC) due to hydrogen embrittlement.[1,3,10–13]

API standard 6ACRA provides acceptable ranges for annealing and ageing heat treatments for 718 in downhole environments, as well as examples of acceptable microstructures and acceptance criteria for room-temperature mechanical properties such as yield strength, ultimate tensile strength, percent elongation, reduction of area and hardness.[24] The heat treatments in the API standard 6ACRA are intended to achieve high strength while also avoiding growth of δ-phase at grain boundaries. The acceptable heat treatment ranges for the 827 MPa (120 ksi) minimum yield strength and 965 MPa (140 ksi) minimum yield strength designations are shown in Table 2.[24] The heat treatments are based on previous research to determine optimal ageing treatments for alloy 718 for use in oil and gas applications.[25] Annealing is performed above 1021°C to ensure dissolution of δ and thereby increases hydrogen embrittlement resistance and the amount of niobium available for γ″ precipitation.[21,23,26,27] Over-ageing near 800°C can produce an alloy with a yield strength above 827 MPa (120 ksi). Under-ageing is potentially promising because it limits the amount of δ-phase that forms during ageing, as can be seen in Fig. 3, and can result in an alloy that reaches the 827 MPa (120 ksi) minimum yield strength designation. The 965 MPa (140 ksi) minimum yield strength requires peak-ageing of the γ′ to reach the higher strength level. The heat treatments outlined in API standard 6ACRA do not necessarily result in alloys with the specified minimum yield strength, so it is important to use the actual strength of the material when comparing hydrogen embrittlement resistance. In certain service conditions, alloy 718 can experience hydrogen embrittlement despite being heat treated according to the API standard 6ACRA due to limited δ-phase precipitation along grain boundaries.[3,4]

In order to provide clarification of the effects of microstructure on SSR hydrogen embrittlement of alloy 718,

Table 1 Testing parameters for SSR hydrogen embrittlement studies in Figs. 1 and 2

First author	Reference number	Solution	Cathodic charging current density or potential	Temperature/°C	Strain rate/s^{-1}	Pre-charge/h
Cassagne	3	0.5 M H_2SO_4	5 mA cm^{-2}	40	2×10^{-7}	–
Foroni	7	0.5 M H_2SO_4	5 mA cm^{-2}	40	1×10^{-6}	–
Huang	8	Synthetic Seawater	−1100 mV vs Ag/AgCl	24	4×10^{-6}	48
McCoy	15	0.5 M H_2SO_4	5 mA cm^{-2}	–	1×10^{-6}	–
Kernion	16	3.5% NaCl	−1100 mV vs Saturated calomel (SCE)	–	4×10^{-6}	–

Table 2 Allowable heat treatments for alloy 718 given in API standard 6ACRA[24]

Alloy	Minimum yield strength designation	Anneal temperature/°C	Anneal time/h	Age temperature/°C	Age time/h
718	827 MPa (120 ksi)	1021–1052	1.0–2.5	774–802	6–8
718	965 MPa (140 ksi)	1021–1052	1.0–2.5	760–802	6–8

Table 3 Composition of nickel-base CRA 718

wt %	Ni	Cr	Nb	Mo	Ti	Al	Co
Alloy 718	53.39	18.44	5.00	2.87	1.02	0.52	0.33
C	**Mn**	**Si**	**P**	**S**	**B**	**Cu**	**Fe**
0.015	0.119	0.075	0.009	0.0004	0.003	0.10	17.99

this paper evaluates the susceptibility of different microstructures of alloy 718 to hydrogen embrittlement using constant SSR testing and *in situ* cathodic hydrogen charging parameters. Four different ageing heat treatments were chosen to assess the effect of grain boundary precipitates produced during ageing and differences in strength produced by volume fraction and size of the primary strengthening precipitates γ′ and γ″. Two different annealing heat treatments were also evaluated to determine the effect of grain size on hydrogen embrittlement susceptibility of a peak-aged condition of alloy 718. Mechanical property ratios for SSR tensile tests performed while cathodic hydrogen charging versus tests performed in an inert environment represent the susceptibility of each microstructure to hydrogen embrittlement and are evaluated with respect to the occurrence and appearance of IGC, transgranular cracking (TGC) and ductile microvoid coalescence (MVC) in the fracture surfaces of specimens tested in the hydrogen-rich environment.

Experimental methods

Alloy 718 with the composition given in Table 3 was hot-rolled to a plate with a thickness of 1.91 cm (0.75 in) and a width of approximately 23 cm (9 in). The plate was sectioned and furnace heat-treated according to Table 4. The highest allowed annealing time and temperature within the guidelines of API standard 6ACRA (1050°C for 2.5 h) were chosen for the first four heat treatments to ensure maximum dissolution of δ-phase. An annealing treatment with the lowest allowable temperature in API standard 6ACRA, 1021°C, and shortest allowable time, 1 h, was also performed to produce a condition with a considerably smaller grain size. After annealing, the plates were water quenched to room temperature. Four different ageing treatments were performed to assess the effect of microstructure on hydrogen embrittlement resistance:

(i) A peak-ageing heat treatment was performed on the small and large grain size conditions with the lowest ageing temperature and time allowable in the API standard 6ACRA, 760°C for 6 h.[24]

(ii) An over-ageing heat treatment was performed on the large grain size condition with the highest ageing temperature and time allowable in the API standard, 802°C for 8 h.[24]

(iii) An under-aged condition was produced with the large grain size condition to inhibit δ-phase precipitation at a low ageing temperature of 710°C. Also, the size and volume fraction of the γ′ and γ″ precipitates are likely different from the peak-aged and over-aged conditions.

(iv) A high δ condition with the large grain size was double-aged with a 950°C, 4 h treatment to produce

Table 4 Heat treating schedule and resulting grain sizes for alloy 718

Condition	Anneal temperature/°C	Anneal time/h	Age temperature/°C	Age time/h	Mean intercept length/μm
Peak-aged	1050	2.5	760	6.0	129 ± 5
Over-aged	1050	2.5	802	8.0	121 ± 8
Under-aged	1050	2.5	710	6.0	132 ± 3
High δ	1050	2.5	950 and 760	4.0 and 6.0	146 ± 7
Small grain size	1021	1.0	760	6.0	57 ± 3

acicular δ-phase at a majority of the grain boundaries followed by a 760°C, 6 h heat treatment. As will be shown in the Results and discussion section, the high δ condition did not have as high of a tensile strength as the peak-aged heat treatment, which was most likely due to the formation of less γ′. The formation of δ-phase decreased the amount of available Nb for γ′ precipitation.

The resulting grain sizes for each heat treatment, measured with the concentric circles method outlined in ASTM standard E-112,[28] are also given in Table 4. Metallographic samples of the five heat treatment conditions were prepared and evaluated through light optical microscopy (LOM) and scanning electron microscopy (SEM). Specimens for LOM and SEM analysis were etched with Kalling's No. 2 etchant. Intragranular carbides and grain boundary precipitates were identified with energy-dispersive spectroscopy.

Tensile specimen blanks were machined from the plates in the longitudinal direction by electrical discharge machining. Sub-size tensile specimens with a gauge length of 25.4 mm (1.00 in) and a gauge diameter of 3.81 mm (0.15 in), as specified in NACE TM0198,[29] were machined from the blanks and polished to a surface finish of 0.254 μm (10 μin). Slow strain rate tensile tests were performed at 21.0°C and at an engineering strain rate of 1.0×10^{-6} s^{-1}. Three tests were performed in the ambient laboratory environment, and three tests were performed with CP of the specimen in an acidic solution for each ageing condition. Cathodic polarisation tests were performed in an acrylic cell with a volume of 0.5 L. The cell and specimen were electrically isolated from the frame with ceramic and polymer washers. The cell was filled with 0.5 M H_2SO_4 and de-aerated with 99.999% pure argon gas. The argon gas was bubbled through the solution at a rate of 28 L h^{-1} (1 ft^3 h^{-1}) to stir the solution throughout the test. Cathodic polarisation was performed at a current density of 5 mA cm^{-2}. Two iridium–tantalum oxide-coated titanium anodes functioned as the counter electrodes and were positioned on opposite sides of the specimen. The electrochemical potential was monitored with a saturated calomel reference electrode (SCE). These environmental testing parameters were chosen based on SSR testing methods frequently used in the oil and gas industry. A constant current density of 5 mA cm^{-2} was chosen so that the rate of the hydrogen production reaction on the specimen would be independent of changes in the pH of the solution over time. This current density corresponds to a cathodic potential of approximately −1.0 V versus SCE.

Fracture surfaces were cleaned with methanol. Fractographic images of the fracture surfaces were taken with a Nikon D70 camera. The fracture surfaces were also evaluated using an FEI Quanta 600i environmental scanning electron microscope and a JEOL 7000 field emission scanning electron microscope. Secondary electron imaging was performed at voltages of 15–20 kV.

Results and discussion

δ Precipitates for heat treatment conditions

Scanning electron microscopy evaluation of grain boundaries revealed small δ-phase platelets in the peak- and over-aged conditions (Fig. 4). The δ-phase precipitates were present at many more grain boundaries and were much larger for the over-aged condition than for the peak-aged condition. Differences in the size and distribution of δ-phase were indistinguishable between the large and small grain size peak-aged conditions. No precipitates were found at the grain boundaries for the under-aged condition. The δ-phase precipitates extended into the grains at many grain boundaries for the high δ condition as shown in the SEM image in Fig. 5*a*. The SEM image of the high δ condition in Fig. 5*b* shows $M_{23}C_6$ carbides, which were also found at grain boundaries in the high δ condition but with significantly less grain boundary coverage than δ-phase.

Slow strain rate results and fracture surfaces

The averages of the mechanical property results from the SSR tests performed in air and with CP for the peak-aged, over-aged, under-aged, high δ and small grain size conditions are given in Table 5. The total elongation, yield stress, ultimate tensile stress (UTS) and reduction in area ratios between the CP condition and the ambient environment for all four microstructural conditions are given in Table 6. Figure 6 shows stress–strain curves for the peak-aged, over-aged, under-aged, high δ and small grain size conditions, respectively. Ductility, as represented by total elongation and reduction in area, was

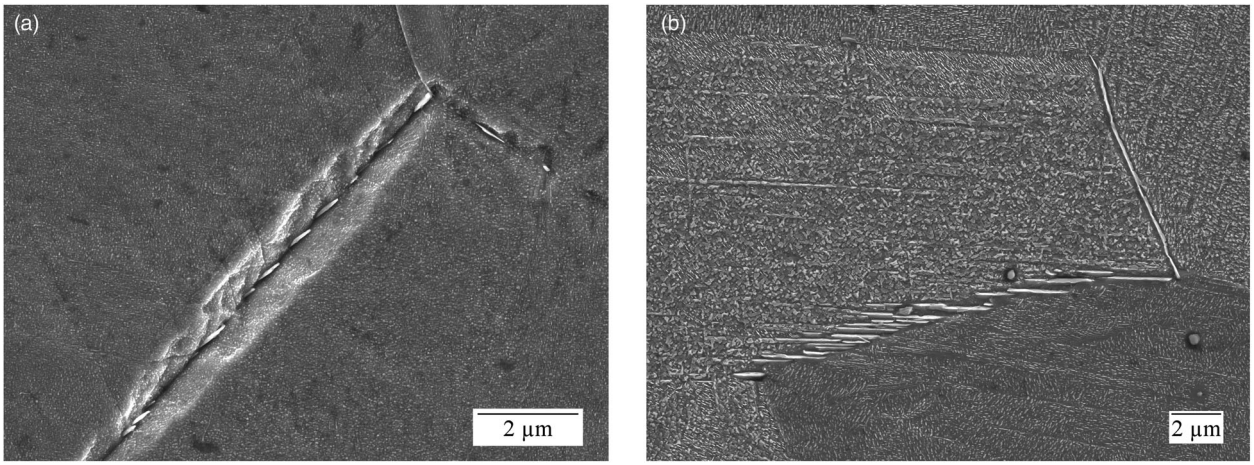

4 Scanning electron microscopy images of grain boundary δ-phase precipitates in *a* peak–aged and *b* over-aged alloy 718

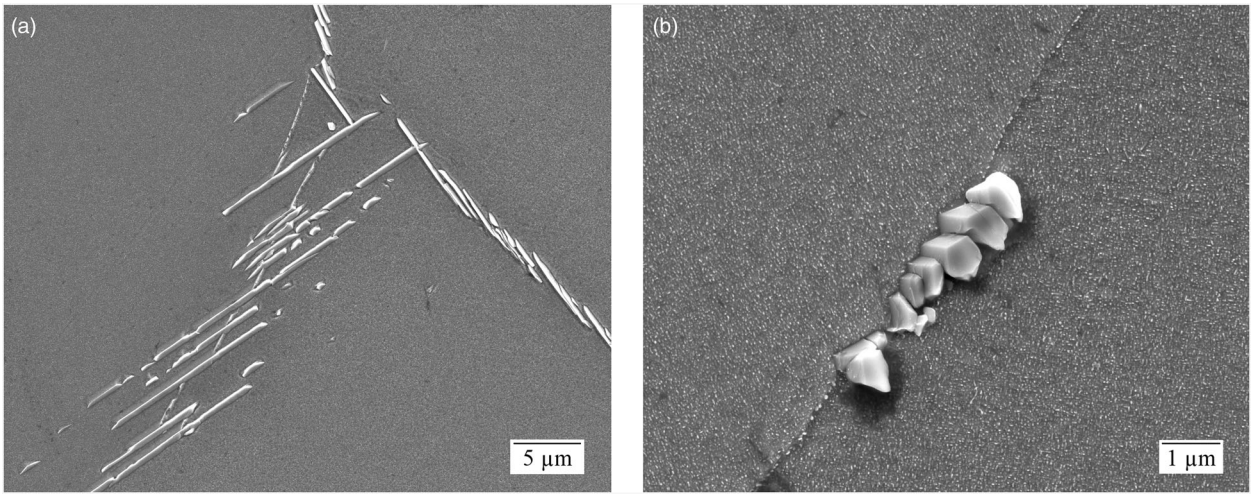

5 Scanning electron microscopy images of *a* grain boundary δ-phase precipitates and *b* $M_{23}C_6$ carbides in high δ alloy 718

Table 5 Strength and ductility results from SSR tests in air and with CP for alloy 718

Condition	Environment	0.2% Yield stress/MPa	UTS/MPa	Total elongation/%	Reduction in area/%
Peak-aged	Air	1006 ± 11	1253 ± 13	28.9 ± 1.6	32.8 ± 2.3
Peak-aged	CP	1000 ± 14	1104 ± 8	3.5 ± 0.6	8.7 ± 0.2
Over-aged	Air	769 ± 14	1166 ± 9	31.2 ± 2.1	32.3 ± 2.8
Over-aged	CP	765 ± 12	947 ± 19	5.8 ± 0.7	9.9 ± 0.4
Under-aged	Air	775 ± 1	1099 ± 13	46.9 ± 2.1	42.8 ± 0.6
Under-aged	CP	770 ± 9	1002 ± 7	21.4 ± 2.3	22.7 ± 0.4
High δ	Air	951 ± 3	1204 ± 2	29.2 ± 1.1	30.3 ± 1.1
High δ	CP	916 ± 3	1042 ± 12	2.3 ± 0.3	7.2 ± 1.4
Small grain size	Air	970 ± 3	1262 ± 8	32.4 ± 2.0	39.5 ± 1.8
Small grain size	CP	965 ± 4	1132 ± 22	4.4 ± 1.2	9.9 ± 2.3

Table 6 Mechanical property ratios for hydrogen-rich environment (CP) versus ambient environment for alloy 718

Condition	Total elongation ratio/%	Reduction in area ratio/%	0.2% Yield stress ratio/%	UTS ratio/%
Peak-aged	12.1 ± 2.1	26.4 ± 1.9	99.4 ± 1.8	88.1 ± 1.1
Over-aged	18.7 ± 2.7	30.8 ± 2.9	99.5 ± 2.5	81.2 ± 1.7
Under-aged	45.6 ± 5.4	53.0 ± 1.3	99.4 ± 1.2	91.2 ± 1.3
High δ	7.9 ± 1.2	23.8 ± 4.7	96.4 ± 0.5	86.5 ± 1.0
Small grain size	13.6 ± 3.9	25.1 ± 6.0	99.6 ± 0.5	89.5 ± 1.9

reduced with hydrogen charging for all microstructural conditions. The yield strength ratios for all conditions were above 96%, indicating that hydrogen had little or no effect on the stress required to initiate plastic deformation. The depth of hydrogen diffusion can be estimated using the diffusion coefficient for hydrogen in alloy 718 at room temperature (2×10^{-15} m^2 s^{-1})[30] and could only have reached approximately 10 μm into the material at yielding due to the slow diffusivity of hydrogen in nickel. The shallowest estimated depth of hydrogen diffusion at failure is for the high δ condition and is approximately 15 μm. The greatest estimated depth of hydrogen diffusion at failure is for the under-aged condition and is approximately 28 μm. Thus, even at failure, hydrogen would only have diffused in the near surface regions of the specimens.

The fracture surfaces of the peak-aged, over-aged, under-aged and small grain size specimens tested in air were ductile. A central fibrous region and shear lips are visible in the macrophotograph of the fracture surface of the small grain size specimen tested in air, shown in Fig. 7*a*; similar fracture surfaces were observed in the peak-aged, over-aged and under-aged conditions. By contrast, the fracture surfaces of the high δ condition tested in air showed ductile fracture mixed with regions of IGC (Fig. 7*b*), a substantially smaller shear lip region and no central fibrous region. However, the high δ condition exhibited similar ductility to the peak-aged, over-aged and small grain size conditions, and the intergranular morphology was associated with ductile microvoid fracture that initiated along the grain boundaries.

When tested in hydrogen, all conditions exhibited both brittle and ductile fracture features. Brittle cracks initiated at the surface and extended into the material until the fracture mechanism transitioned to ductile MVC at the interior of the specimen. The amount of brittle cracking varied between microstructural conditions. The macrophotograph of the fracture surface of the over-aged condition tested in the hydrogen-rich environment in Fig. 8*a* shows a ductile region of MVC and a brittle region composed of IGC and TGC. IGC and TGC in the brittle fracture region of a small grain size specimen tested in

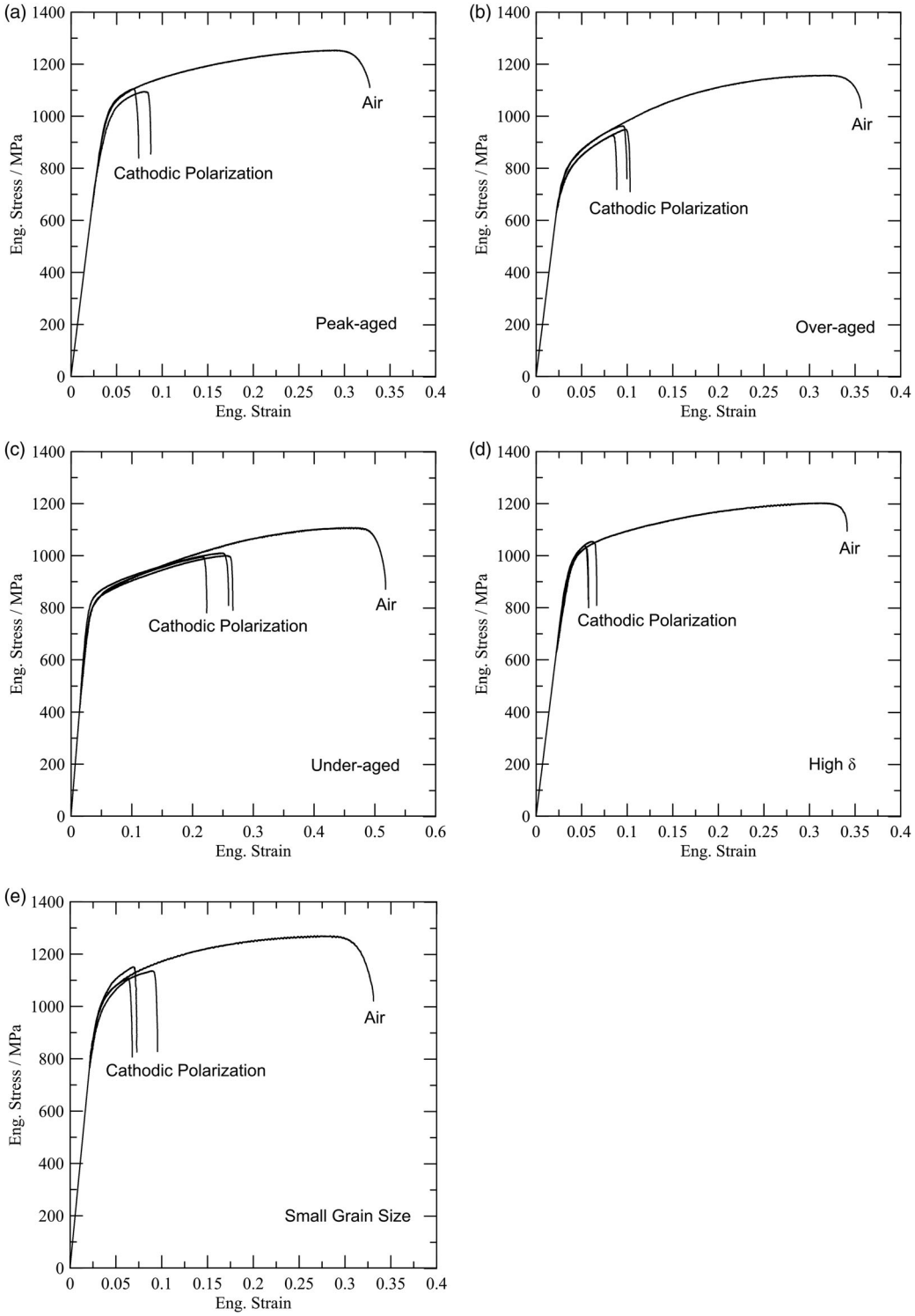

6 Engineering stress versus engineering strain curves for SSR tensile tests in air and under CP for alloy 718 in the *a* peak-aged, *b* over-aged, *c* under-aged, *d* high δ and *e* small grain size conditions. Only one representative stress–strain curve is shown for air

hydrogen are clearly visible in the SEM image in Fig. 8*b*. Transgranular cracking in the peak-aged, over-aged, small grain size and under-aged conditions resembled cleavage on specific crystallographic planes with visible river marks. Scanning electron microscopy images of regions containing TGC and IGC are shown for the small grain size condition in Fig. 8*c* and for the over-aged condition in Fig. 8*d*. Cleavage cracking was sporadically located in the brittle regions and frequently occurred where a smooth intergranular feature intercepted a grain boundary or annealing twin. Fracture features that appeared as deviations from the intergranular crack path were visible in all conditions. These fracture features can be seen in the SEM images in Figs. 8*b–d*.

The results of the peak-aged and over-aged conditions with the large grain size highlight how ageing treatment

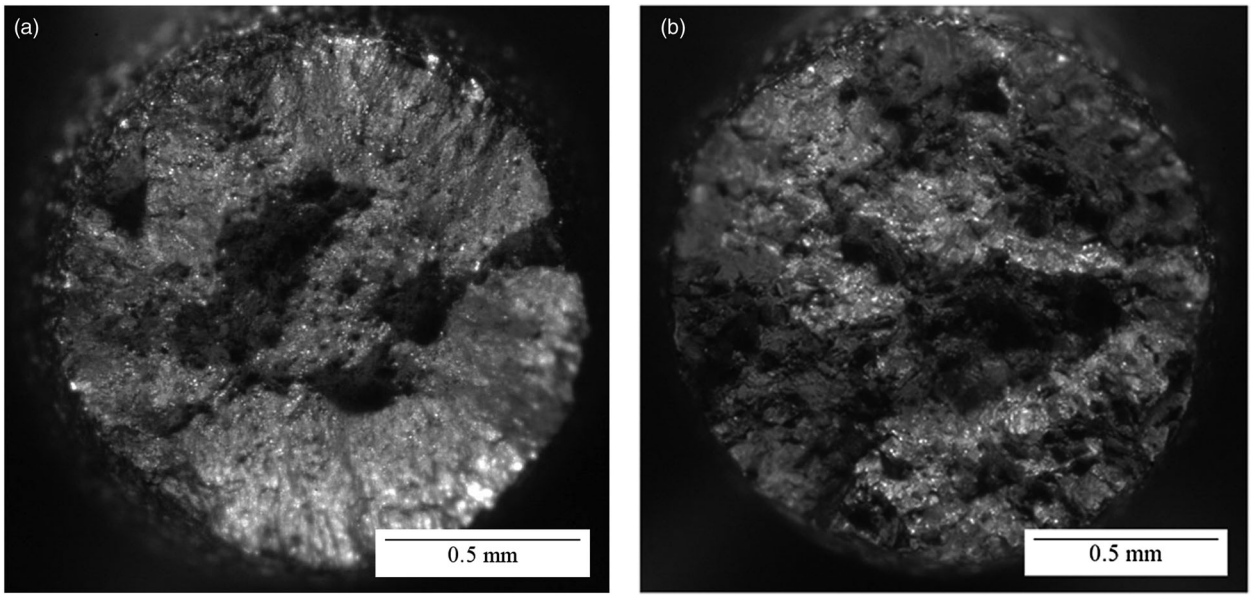

7 Macrophotograph of the fracture surfaces of alloy 718 after SSR testing to failure in air of the *a* small grain size condition and *b* high δ condition

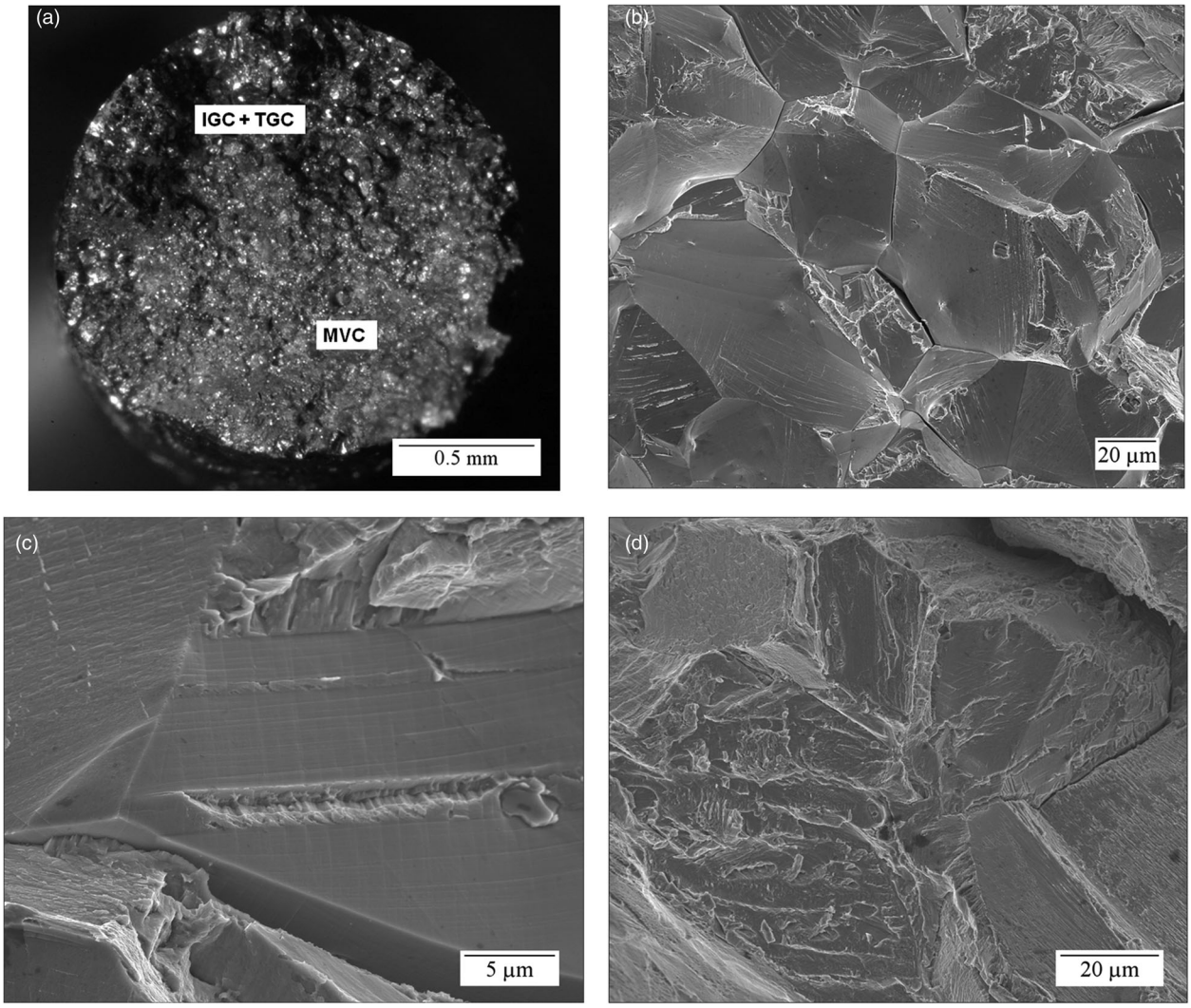

8 *a* Macrophotograph of the fracture surface of the over-aged condition of alloy 718 SSR tested under CP showing regions of IGC, TGC and ductile MVC. *b* Scanning electron microscopy image of the brittle fracture region of the small grain size condition of alloy 718 tested under CP. *c* Scanning electron microscopy image of TGC that occurred along specific crystallographic planes mixed with smooth IGC of the small grain size condition of alloy 718. *d* Scanning electron microscopy image of IGC and TGC in the over-aged condition of alloy 718 SSR tested under CP. Fracture features that appear as deviations from smooth IGC are visible in *b–d*

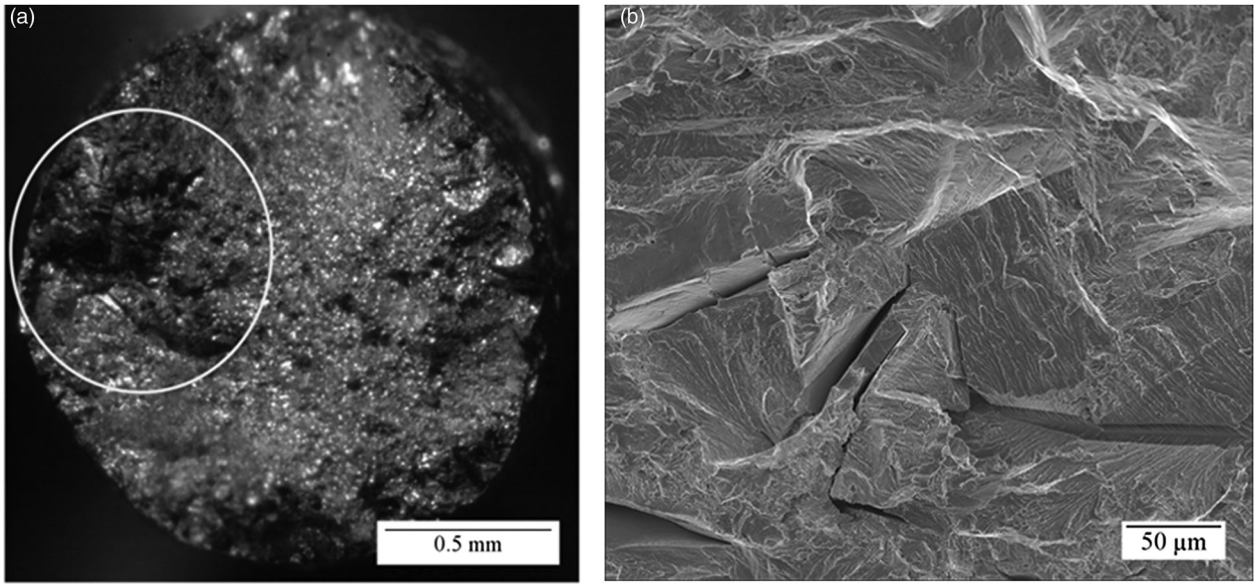

9 ***a*** **Macrophotograph highlighting a small region of brittle fracture visible on the fracture surface of the under-aged condition of alloy 718 tested in hydrogen and** ***b*** **SEM image of the brittle crack region showing a combination of TGC, IGC and some ductile fracture**

affects hydrogen embrittlement susceptibility and are industrially relevant because they conform to API standard 6ACRA. The over-aged condition exhibited a greater total elongation ratio (18.7%) and reduction in area ratio (30.8%) than the peak-aged condition (12.1% total elongation ratio and 26.4% reduction in area ratio). On the other hand, the ultimate tensile strength ratio for the over-aged condition (81.2%) is lower than the ultimate tensile strength ratios for all other conditions because of the higher work hardening rate for the over-aged condition. That is, the loss of plastic deformation due to premature failure in hydrogen prevents the greater increase in stress from work hardening that the over-aged condition experiences compared with the other conditions.

The ratio of total elongation in the hydrogen-rich environment versus the ambient environment for the under-aged condition (45.6%) was significantly greater than that for any other conditions. A macrophotograph of the fracture surface of the under-aged condition tested in hydrogen is shown in Fig. 9*a*, and the main region of brittle fracture is highlighted. The under-aged condition exhibited less brittle fracture than any of the other conditions when tested in hydrogen. There were a few additional short brittle cracks at the edges of the fracture surface, and the cracks were all connected by ductile MVC. The SEM image of the fracture surface of the under-aged condition tested in hydrogen in Fig. 9*b* shows more TGC and MVC and much less IGC in the brittle region compared with the brittle regions of the other conditions. The smaller amount of IGC may be due to the lack of δ-phase at the grain boundaries unlike the other conditions. The correlation between better ductility and less IGC in the under-aged condition suggests that fast, brittle cracking occurs more readily through the conditions containing δ-phase on the grain boundaries.

The high δ condition had the lowest total elongation ratio (7.9%), which was expected due to the high amounts of grain boundary precipitates (acicular δ-phase and $M_{23}C_6$ carbides). The macrophotograph of the fracture surface of the high δ condition SSR tested in hydrogen in Fig. 10*a* shows a greater amount of brittle fracture than for any other conditions. The brittle fracture of the high δ condition was composed entirely of IGC, which transitioned to ductile fracture at the centre of the specimen. The higher magnification SEM image of the brittle region of the high δ condition in Fig. 10*b* shows a serrated pattern on the intergranular facets, which differs from the smooth intergranular facets of the other conditions. This morphology is most likely due to the cracks propagating along the δ-phase at the grain boundaries. The increase in δ-phase, and potentially to a lesser extent $M_{23}C_6$, likely facilitated IGC in hydrogen, which resulted in a larger amount of brittle cracking, no TGC, and a decrease in tensile elongation and reduction in area. The greater amount of TGC for the more ductile under-aged condition and the complete lack of TGC for the high δ condition may show that hydrogen cracks prefer to propagate along grain boundaries with δ-phase but propagate more transgranularly when susceptible grain boundaries are not present.

The small grain size condition and the peak-aged condition had the same ageing heat treatment, but the grain size of the peak-aged condition (129 μm) was about twice the grain size of the small grain size condition (57 μm) due to the different annealing treatments. The smaller grain size condition exhibited a slightly better total elongation ratio (13.6%) than the peak-aged condition (12.1%) but a slightly worse reduction in area ratio (25.1% versus 26.4%). The reduction in area in air for the small grain size condition was well above the peak-aged condition, which may contribute to the lower reduction in area ratio. The total elongation and reduction in area ratios were within one standard deviation of each other, so the difference between the ductility ratios of the two conditions are not considered statistically significant. An increase in hydrogen embrittlement resistance due to a smaller grain size for alloy 718 has been attributed to the potential for a lower concentration of

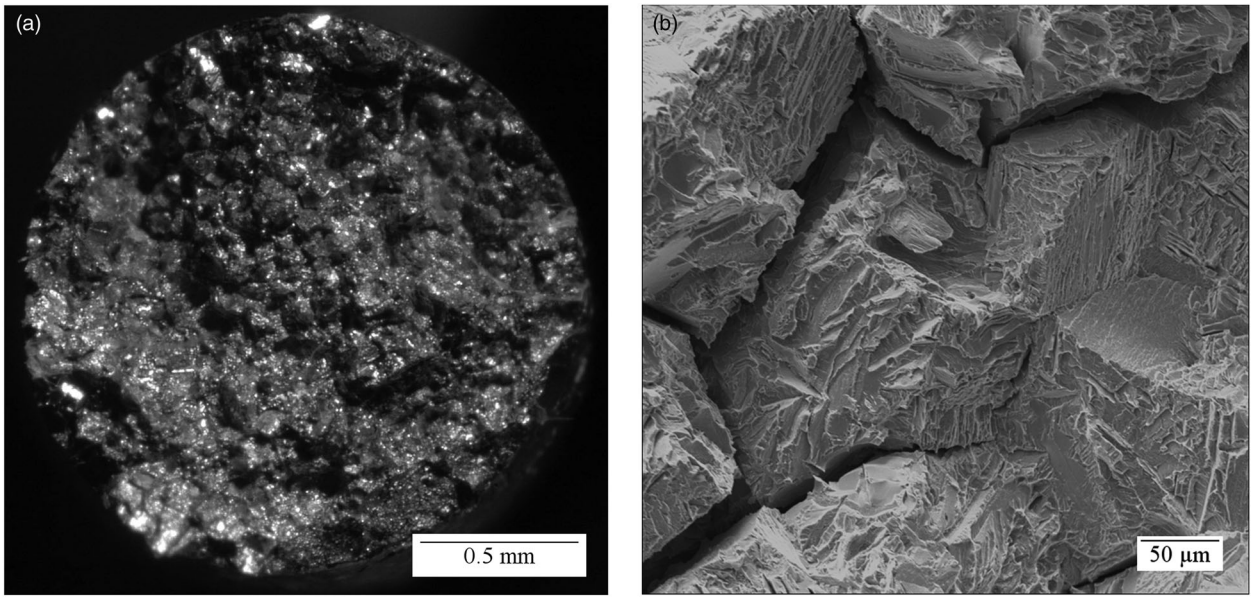

10 ***a*** **Macrophotograph showing extensive IGC with some ductile fractures on the fracture surface of high δ alloy 718 SSR tested in hydrogen and** ***b*** **SEM image showing serrated morphology on IGC facets**

impurities at the grain boundaries for a smaller grain size;[31] however, the peak-aged conditions with two different grain sizes studied here showed no statistical difference in hydrogen embrittlement susceptibility, which corresponds to the similarity in fracture appearance as well as the presence of small δ-phase precipitates at the grain boundaries of both conditions.

All specimens tested in air exhibited orange peel along the gauge length with no visible surface cracking. When tested in the hydrogen-rich environment, all conditions exhibited surface cracking on the gauge length, mostly concentrated near the fracture surface. The macrophotograph in Fig. 11 shows surface cracking along the gauge length near the fracture for the high δ condition tested in hydrogen. The high δ condition appeared to have the most surface cracking, while the under-aged condition had the least.

The differences in hydrogen embrittlement susceptibility of alloy 718 are influenced by both grain boundary precipitates and the volume fraction and size of the γ′ and γ″ primary strengthening phases. Differences in γ′ and γ″ are evident when comparing the strength levels of the different heat treatment conditions and the work hardening behaviour, which is affected by size and coherency of the precipitates. A plot of the total elongation ratios versus yield strengths for all heat treatment conditions of alloy 718 is shown in Fig. 12*a*. The under- and over-aged conditions have almost identical yield strengths, but the under-aged condition has vastly superior hydrogen embrittlement resistance. The lack of grain boundary precipitates in the under-aged condition probably had a significant effect on the greater hydrogen embrittlement resistance of that condition, as evidenced by the TGC in the brittle region of the specimens tested with CP. Though the under- and over-aged conditions had similar yield strengths, the over-aged condition had a higher ultimate tensile strength, which is attributed to differences in γ′ and γ″ volume fraction and size and could also have a role in the difference in hydrogen embrittlement resistance.

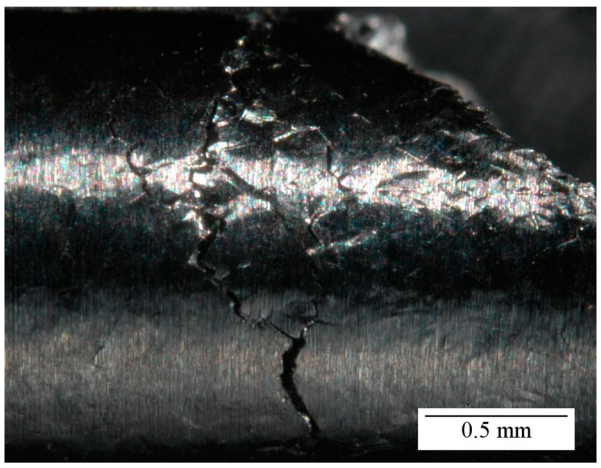

11 Macrophotograph of surface cracking in the vicinity of the fracture of high δ alloy 718 after SSR test with CP

The over-aged condition had greater hydrogen embrittlement resistance than the peak-aged condition despite the larger size and amount of grain boundary δ-phase. Besides the grain boundary precipitates, the other main difference between the over- and peak-aged condition is the volume fraction and size of the γ′ and γ″ primary strengthening phases, which therefore likely also affects the hydrogen embrittlement susceptibility of alloy 718. The over-aged condition has a much higher work hardening rate than the other conditions, which implies that it contains larger and possibly less coherent precipitates.[32]

Figure 12*b* shows a plot of the total elongation ratios versus ultimate tensile strengths for all heat treatment conditions of alloy 718. Differences in strength are almost entirely due to changes in γ′ and γ″, and the hydrogen embrittlement susceptibility tends to increase with the increasing ultimate tensile strength. Above an ultimate tensile strength of 1200 MPa, there is no clear correlation between strength and ductility ratios for the peak-aged conditions, which is most likely due to microstructural

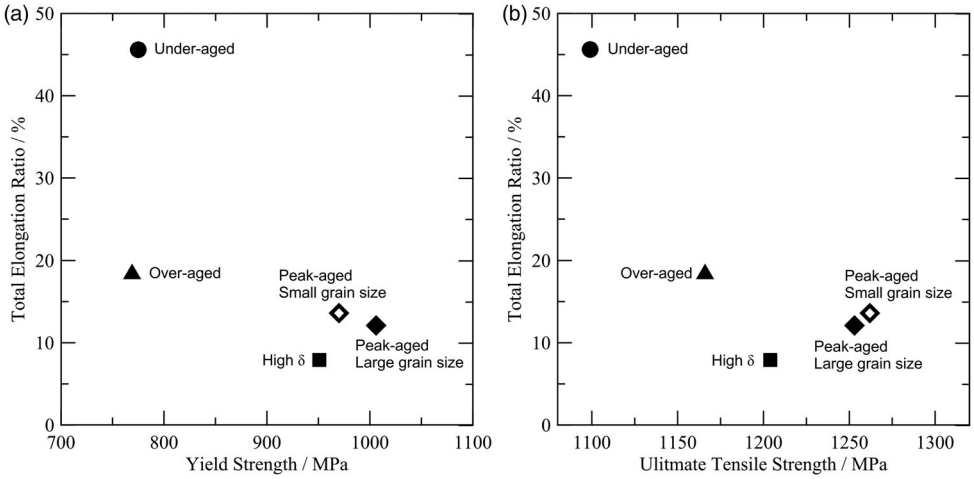

12 Total elongation ratio (%) versus *a* yield strength (MPa) and *b* ultimate tensile strength (MPa) for all heat treatment conditions of alloy 718

differences other than the ageing of the γ′ and γ″. The lower strength level of the high δ condition compared with the other peak-aged conditions is most likely the result of δ-phase precipitation during the first ageing step decreasing the amount of available Nb for precipitation of γ″. Changes in grain size had very little effect on the strength level and hydrogen embrittlement susceptibility of the peak-aged condition.

In addition to microstructural differences, hydrogen embrittlement susceptibility determined by SSR testing may be affected by the stress imposed on cracks during plastic deformation, which depends on the yield stress and work hardening rate of the alloys. There is a larger stress driving crack propagation for alloys with higher strengths, which could affect the speed of crack propagation during the SSR test.

Clearly, the hydrogen embrittlement susceptibility of alloy 718 is affected by both grain boundary precipitation and γ′ and γ″ volume fraction and/or size, as best evidenced by the over-aged condition which had inferior hydrogen embrittlement resistance compared with the under-aged condition, even though both conditions had almost identical yield strengths, and superior hydrogen embrittlement resistance compared with the peak-aged condition despite having more grain boundary δ-phase. Further investigation is required to determine the effect of differences in γ′ and γ″ volume fraction and size on the mechanism of hydrogen embrittlement in alloy 718.

Summary and conclusions

Slow strain rate tensile tests were performed on peak-aged, over-aged, under-aged, high-δ and small grain size conditions of alloy 718 in air and under CP to assess their susceptibility to hydrogen embrittlement. The under-aged condition exhibited superior hydrogen embrittlement resistance compared with all other conditions. The greater hydrogen embrittlement resistance of the under-aged condition is likely attributed to the lack of δ-phase at the grain boundaries, which resulted in a brittle region of mostly TGC and limited IGC. The high δ condition, with extensive precipitation of δ-phase at the grain boundaries, exhibited the lowest hydrogen embrittlement resistance and a fracture surface with a brittle region entirely composed of intergranular fracture with a serrated appearance on the facets. Generally, hydrogen embrittlement resistance increased with a decreasing amount of grain boundary δ-phase except that the over-aged condition had slightly better resistance than the peak-aged conditions despite having slightly more and larger δ-phase precipitates. The peak- and over-aged condition results suggest that γ′ and γ″ volume sizes and/or fraction have an influence on hydrogen embrittlement resistance of alloy 718 in addition to a possible influence of alloy strength. Also, a decrease in grain size had no effect on hydrogen embrittlement resistance and fracture appearance in the hydrogen-rich environment. Despite differences in hydrogen embrittlement resistance, the peak-aged, over-aged, high δ and small grain size conditions all had a similar ductile fracture mode in the ambient environment; however, the high δ condition exhibited IGC in the ambient environment due to microvoids forming along the grain boundaries.

Acknowledgements

The authors gratefully acknowledge the support of the Advanced Steel Processing and Products Research Center at the Colorado School of Mines as well as the experimental and material support of the Special Metals Corporation and Chevron Corporation.

ORCID

B. Kagay http://orcid.org/0000-0003-2709-6324

References

1. S. Huizinga, B. McLoughlin, J. Jong and W. Like: 'Offshore nickel alloy tubing hanger and duplex stainless steel piping failure investigations', Proc. Conf. Corrosion, 2003, National Association of Corrosion Engineers, Paper 03129, 1–9.
2. S. Shademan, J. Martin and A. Davis: 'UNS N07725 nickel alloy connection failure', Proc. Conf. Corrosion, 2012, National Association of Corrosion Engineers, 1–23.
3. T. Cassagne, M. Bonis, D. Hillis and C. Duret: 'Understanding field failures of alloy 718 forging materials in HP/HT wells', Proc. Conf. Eurocorr, 2008, 1–13.

4. P. I. Nice, E. Piccolo, R. Morana and L. Scoppio: 'Corrosion evaluation of temporarily installed 'Well Zone Isolation Equipment' after long term exposure to a caesium formate mud system in a North Sea HPHT well', Proc. Conf. Corrosion, 2013, National Association of Corrosion Engineers, Paper 2313, 1–15.
5. E. Piccolo, P. I. Nice, O. Fattnes, R. Morana, A. Bufalini, A. Lucci and L. Scoppio: 'High pressure high temperature testing of PH nickel alloy and super martensitic stainless steel in cesium formate Completion Fluid', Proc. Conf. Corrosion, 2012, National Association of Corrosion Engineers, 1–12.
6. P. R. Rhodes: 'Environment-assisted cracking of corrosion-resistant alloys in oil and gas production environments: A review', *Corrosion*, 2001, **57**, (11), 923–966.
7. L. Foroni and C. Malara: 'Hydrogen embrittlement susceptibility of precipitation hardened Ni-alloys', Proc. Conf. Corrosion, 2014, National Association of Corrosion Engineers, Paper 3948, 1–15.
8. W. Huang, W. Sun, A. Samson, D. Muise and C. Haarseth: 'Investigation of hydrogen embrittlement susceptibility of precipitation hardened nickel alloys under cathodic protection condition', Proc. Conf. Corrosion, 2014, National Association of Corrosion Engineers, Paper 4248, 1–15.
9. P. Nice, G. Rorvik, R. Strong, J. H. Olsen, W. M. Bailey and T. G. Mobberley: 'Hydrogen embrittlement failure of a precipitation hardened nickel alloy subsurface safety valve component installed in a North Sea Seawater injection well', Proc. Conf. Corrosion, 2014, National Association of Corrosion Engineers, Paper 3892, 1–16.
10. F. Pires, R. Clements, F. Santos, J. Clevelario and T. Sheldrake: 'Evaluation of the performance of inconel 718 fasteners subjected to cathodic protection systems in offshore and subsea applications', Proc. 30th Int. Conf. on 'Ocean, Offshore and Arctic Engineering', 2011, American Society of Mechanical Engineers, 165–172.
11. T. S. Rosa, A. F. Ribeiro, L. H. de Almeida and D. S. dos Santos: 'Effects of the microstructure on the hydrogen diffusivity in Ni-based superalloy 718', *Defect Diffus. Forum*, 2010, **297–301**, 733–738.
12. L. Liu, C. Zhai, C. Lu, W. Ding, A. Hirose and K. F. Kobayashi: 'Study of the effect of δ phase on hydrogen embrittlement of inconel 718 by notch tensile tests', *Corr. Sci.*, 2005, **47**, (2), 355–367.
13. L. Liu, K. Tanaka, A. Hirose and K. F. Kobayashi: 'Effects of precipitation phases on the hydrogen embrittlement sensitivity of inconel 718', *Sci. Technol. Adv. Mater.*, 2002, **3**, (4), 335–344.
14. L. Fournier, D. Delafosse and T. Magnin: 'Cathodic hydrogen embrittlement in alloy 718', *Mater. Sci. Eng.: A*, Aug. 1999, **269**, (1–2), 111–119.
15. S. A. McCoy, S. K. Mannan, C. S. Tassen, D. Maitra and J. R. Crum: 'Investigation of the effects of hydrogen on high strength precipitation hardened nickel alloys for O&G service', Proc. Conf. Corrosion, 2015, National Association of Corrosion Engineers, Paper 5911, 1–10.
16. S. J. Kernion, K. A. Heck, J. H. Magee and T. N. Werley: 'Effect of microstructure and processing on the hydrogen embrittlement of Ni-base superalloys', Proc. Conf. Corrosion, 2015, National Association of Corrosion Engineers, Paper 6053, 1–12.
17. A. Oradei-Basile and J. F. Radavich: 'A current TTT diagram for wrought alloy 718', Proc. Conf. on 'Superalloys 718,625 and various derivatives', 1991, The Minerals, Metals, and Materials Society, 325–335.
18. H. Eiselstein: 'Metallurgy of a columbium-hardened nickel–chromium–iron alloy', STP 369 advances in the technology of stainless steels and related alloys, ASTM International, 1965, 65–79.
19. W. Boesch and H. Canada: 'Precipitation reactions and stability of Ni3Cb in inconel alloy 718', Proc. Conf. 1968 Seven Springs Int. Symp., 1968, 579–596.
20. J. W. Brooks and P. J. Bridges: 'Metallurgical stability of inconel 718', Proc. Conf. Superalloys 1988 Symp., 1988, 33–42.
21. X. Xie, C. Xu, G. Wang, J. Dong, W. Cao and R. Kennedy: 'TTT diagram of a newly developed nickel-base superalloy – ALLVAC 718 plus', Proc. Conf. on 'Superalloys 718, 625, 706 and derivatives', 2005, The Minerals, Metals, and Materials Society, 193–202.
22. M. J. Donachie and S. J. Donachie: 'Superalloys: A technical guide'; 2002, Materials Park, OH, ASM International.
23. X. Wei, W. Zheng, Z. Song, T. Lei, Q. Yong and Q. Xie: 'Elemental partitioning characteristics of equilibrium phases in inconel 718 alloy at 600–1100°C', *J. Iron Steel Res. Int.*, 2013, **20**, (6), 88–94.
24. 'Age-hardened nickel-based alloys for oil and gas drilling and production equipment', 6ACRA, API, Washington, DC, USA, 2015.
25. R. B. Bhavsar, A. Collins and S. Silverman: 'Use of alloy 718 and 725 in oil and gas industry', Proc. Conf. on 'Superalloys 718, 625, 706 and various derivatives', 2001, The Minerals, Metals, and Materials Society, 47–55.
26. D. Cai, W. Zhang, P. Nie, W. Liu and M. Yao: 'Dissolution kinetics of δ phase and its influence on the notch sensitivity of inconel 718', *Mater. Characterization*, 2007, **58**, (3), 220–225.
27. S. Azadian, L. Wei and R. Warren: 'Delta phase precipitation in inconel 718', *Mater. Charact.*, 2004, **53**, 7–16.
28. 'Standard test methods for determining average grain size'; 1996, West Conshohocken, PA, E112, ASTM.
29. 'NACE standard slow strain rate test method for screening corrosion-resistant alloys (CRAs) for stress corrosion cracking in sour oilfield service'; 2004, Houston, TX, TM0198, NACE International.
30. B. Pound: 'Hydrogen trapping in precipitation-hardened alloys', *Acta Metall. Mater.*, 1990, **38**, (12), 2373–2381.
31. J. Lillard, R. Kelly and R. Gangloff: 'Effect of electrode potential on stress corrosion cracking and crack chemistry of a nickel-base superalloy', Proc. Conf. Corrosion, 1997, National Association of Corrosion Engineers, 1–26.
32. G. Dieter: 'Mechanical metallurgy', 3rd edn, 212–220; 1986, New York, McGraw-Hill.